Synthesis of CuO$_x$/TiO$_2$ Photocatalysts with Enhanced Photocatalytic Performance

Li Li,* Xinhong Chen, Xuejun Quan, Facheng Qiu, and Xingran Zhang

ACCESS | ᵘ̲ᵘ̲ᵘ̲ Metrics & More | 📖 Article Recommendations | ˢⁱ Supporting Information

ABSTRACT: CuO$_x$/TiO$_2$ co-photocatalysts with various Cu loading contents were synthesized by an impregnation method, and their photocatalytic activities were evaluated by photodegradation of organic pollutants under visible light illumination. The as-prepared CuO$_x$/TiO$_2$ composites exhibited a unique structure, in which CuO$_x$ clusters with about 2−3 nm nanocrystals were uniformly distributed on the TiO$_2$ cube. The mesoporous Ti^{3+}/TiO$_2$ substrate with a uniform pore structure greatly improved the uniformity of the loaded Cu, wherein Ti^{3+} acted as a reducing agent for reducing Cu^{2+} to Cu$^+$ and Cu^0. The reversible process of the Cu species between Cu$^+$ and Cu^0 markedly enhanced the photocatalytic activity of the CuO$_x$/TiO$_2$ co-photocatalyst, by promoting the transfer of photogenerated electrons and suppressing the recombination of photogenerated electron and hole pairs. The synergistic effect between CuO$_x$ and TiO$_2$ also played an important role in enhancing the photocatalytic activity of the CuO$_x$/TiO$_2$ co-photocatalyst. The results indicated that CuO$_x$/TiO$_2$-1 had the highest photocatalytic efficiency, which was 1.5 times higher than that of the commercial nano-TiO$_2$ P25 under visible light, and demonstrated a good stability even after five recycles. This structural design and the valence control strategy for the Cu atom provide an idea that facilitates the utilization of visible light and the improvement of the photocatalytic activity of TiO$_2$, promoting the practical application of the TiO$_2$ photocatalyst.
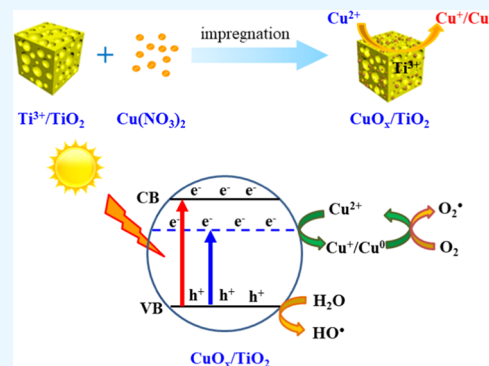
1. INTRODUCTION

Due to its wide band gap (3.2 eV) and higher recombination of charge carries, in practical applications, pure titanium dioxide (TiO$_2$) has low solar efficiency and quantum efficiency; hence, it is not a good photocatalyst.[1−3] In recent years, much effort has been focused on enhancing the photocatalysis efficiency.[4,5] One approach is to improve the specific surface area and surface-active site of TiO$_2$ by changing its crystal size, exposure crystal plane, and surface morphology, which is conducive to the transfer and diffusion of reactants and products.[6−8] Another approach is to dope various transition metal cations, non-metal elements, or other semiconductor materials, which results in the light response changing from UV irradiation to visible light.[9,10] The doped metal cations can act as efficient electron traps based on the charge transfer mechanism, inhibiting the photoelectron−hole pair recombination and improving the photoluminescence quantum yields.[11−14] In particular, doping noble metal nanoparticles can improve the photocatalytic activity of TiO$_2$ efficiently owing to its excellent resistance of oxidation, the surface plasmon resonance (SPR) effect will be generated on the surface of noble metal nanoparticles, and the effective transport of electrons from the metal particles to the TiO$_2$ conduction band will be promoted. Therefore, immense efforts have been devoted to studying both theoretically and experimentally the photo-activity of TiO$_2$ by doping noble metals.

Compared with Au, Pt, Pd, Rh, Ru, Ag, and other precious metals, the transition metal Cu is suitable for large-scale commercial applications owing to its cost effectiveness.[15−19] Since the ionic radius of Cu^{2+} (0.073 nm) is close to that of Ti^{4+} (0.068 nm), the loaded Cu can enter the TiO$_2$ matrix by occupying the position of the Ti atom.[20−23] When the TiO$_2$ surface is loaded with copper, it will introduce the d intermediate state to form an intermediate energy level, which functions as "charge carrier traps" and broadens the spectrum response range.[24,25] It is beneficial to improve the separation efficiency of the photogenerated electron−hole pairs. Docao et al.[21] synthesized Cu-loaded TiO$_2$ by a wet impregnation method using copper acetate monohydrate as a precursor. Under AM 1.5 sunlight irradiation, Cu/TiO$_2$ can effectively split water vapor to produce H$_2$ and O$_2$, which is an important method to convert solar energy into chemical energy. Lee et al.[20] synthesized a site-specific single-atom Cu/TiO$_2$ photocatalyst by a hard template method. Through an atomic-level design and synthesis strategy, the Cu/TiO$_2$
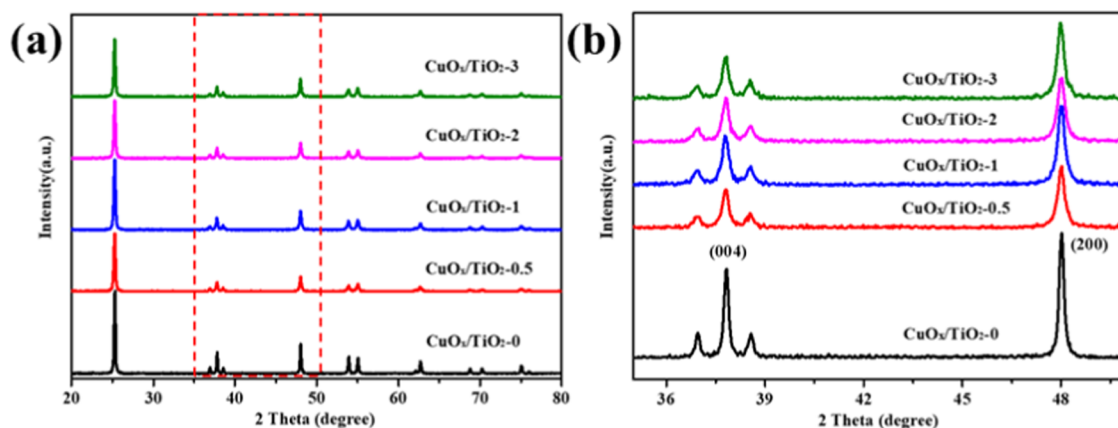
Figure 1. (a, b) XRD patterns of the CuO_x/TiO_2 samples.

catalyst showed a reversible and cooperative photoactivation process, with reversible photoelectric performance and enhanced photocatalytic hydrogen production activity. In addition, copper is an excellent antibacterial agent. Doping Cu into the TiO_2 matrix has dual advantages; it not only can reduce the recombination of electron−hole pairs but also can realize antibacterial and antiviral functions, which promote the application of TiO_2 composite materials in photocatalysis, biomedicine, and antibacterial coatings.[25]

From the perspective of green chemistry that focuses on the synthesis of an environmentally friendly photocatalyst, a cooperative photoactivation process for enhancing the photocatalysis performance is imperatively demanded. To date, a variety of high-performance visible light catalysts have been synthesized through combining element loading and special configurations (mesoporous, hollow, oxygen vacancies) together, to realize a cooperative photoactivation process, and applied in photocatalysis, biocatalysis, and new energy storage.[26−29] Park et al.[30] synthesized a $Cu_xO−TiO_2$ photocatalyst in a simple way, which showed high CO_2 photoreduction efficiency due to the mesoporous p-type/n-type heterojunction structure. In addition, porous materials have a large specific surface area and uniform pore structure, which are conducive to the diffusion of the metal precursor solution and uniform loading at the molecular level. Li et al.[31] reported a sol−gel method to synthesize a mesoporous silica-supported Cu/TiO_2 co-catalyst, which had a high surface area (300 $m^2 \cdot g^{-1}$) and exhibited enhanced CO_2 photoreduction ability, and the quantum yield reached 1.41%. Although the metal was not loaded on the mesoporous TiO_2 with a defective structure, this approach could offer potential advantages compared with the pure TiO_2-loaded metal co-catalyst.

In this paper, we used Ti^{3+}/TiO_2 powder synthesized earlier as the substrate to synthesize CuO_x/TiO_2 by an impregnation method. The CuO_x/TiO_2 had a special configuration that offers several advantages for photocatalytic application owing to its defective structure. In the process of loading CuO_x, the uniform pore structure and high specific surface area of mesoporous Ti^{3+}/TiO_2 particles are conducive to the uniform loading of Cu^{2+}, and Ti^{3+} is used as a reducing agent to reduce Cu^{2+} to Cu^+ partially. With these unique configurations, CuO_x/TiO_2 can be expected to be a more effective alternative to remove organic pollutants in aqueous solution, such as rhodamine B.

2. EXPERIMENTAL SECTION

2.1. Materials. Titanium sulfate $(Ti(SO_4)_2)$ and oxalic acid $(H_2C_2O_4)$ were obtained from Sinopharm Chemical Regent Co., Ltd. (Shanghai, China). Copper nitrate $(Cu(NO_3)_2 \cdot 2H_2O)$, copper sulfate $(CuSO_4 \cdot 5H_2O)$, copper acetate monohydrate $(Cu(CH_3COO)_2 \cdot H_2O)$, and rhodamine B (RhB) were all obtained from Chengdu Ke Long Regent Co., Ltd. (Chengdu, China). Nano-TiO_2 (P25) was obtained from Degussa (75% anatase and 25% rutile). They were all used directly without any further treatment. The water used in the experiments was double-distilled water.

Table 1. Physical Properties of the CuO_x/TiO_2 Sample

samples	crystal size(nm)	a, b (Å)	c (Å)	band gap (eV)
CuO_x/TiO_2-0	41.1	3.7865	9.4993	2.92
CuO_x/TiO_2-0.5	41.7	3.7884	9.5009	2.90
CuO_x/TiO_2-1	47.4	3.7877	9.5022	2.88
CuO_x/TiO_2-2	48.9	3.7875	9.5045	2.87
CuO_x/TiO_2-3	45.3	3.7891	9.5069	2.84

2.2. Synthesis. According to the hydrothermal method reported by the research group,[32] Ti^{3+} self-doped TiO_2 was synthesized using $Ti(SO_4)_2$ as a precursor and oxalic acid as a reducing agent. CuO_x/TiO_2 was prepared by the wet impregnation method. A total of 0.2 g of Ti^{3+}/TiO_2 powder was dispersed in 20 mL of H_2O and ultrasonically treated for 20 min. Then, a certain amount of copper nitrate (the mole ratio of the amount of Cu to TiO_2 ranging from 0.5, 1.0, and 2.0 to 3.0%) was added and stirred in a water bath kept at 90 °C for 2 h. The obtained solution was dried at 80 °C for 12 h and then calcined at 400 °C for 4 h under an air atmosphere. The samples obtained under different conditions are denoted as CuO_x/TiO_2-N, where N refers to the mole ratio of the amount of Cu to TiO_2.

2.3. Characterization. The XRD pattern was recorded using an X-ray diffractometer (EMPYREAN, Panalytical) with Cu Kα radiation. The morphology and crystal size of the sample were characterized by transmission electron microscopy (TEM, Talos F200S, Thermo Fisher). The crystal phase was measured by Raman spectroscopy (LabRAM HR Evolution, HORIBA Jobin Yvon S.A.S.) with an Ar ion laser source. The UV−vis diffuse reflection spectra were obtained with $BaSO_4$ as a reference using ultraviolet−visible light (UV−vis) spectroscopy (TU-1901, PERSEE). The specific surface
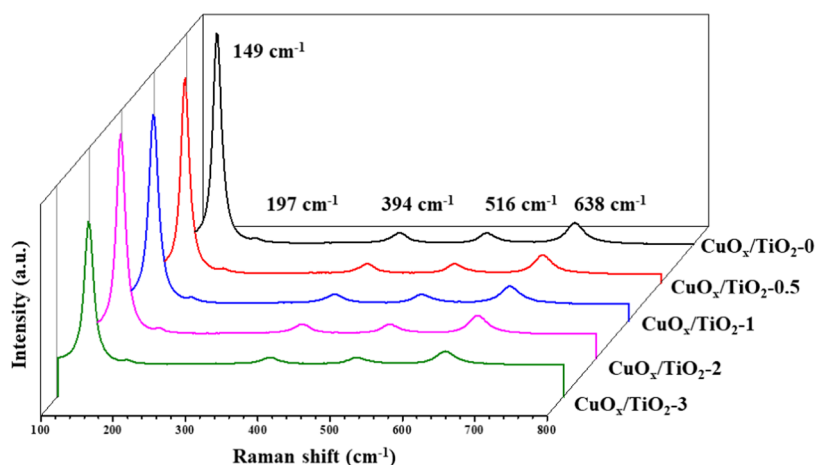
Figure 2. Raman scattering spectra of the CuO_x/TiO_2 samples.

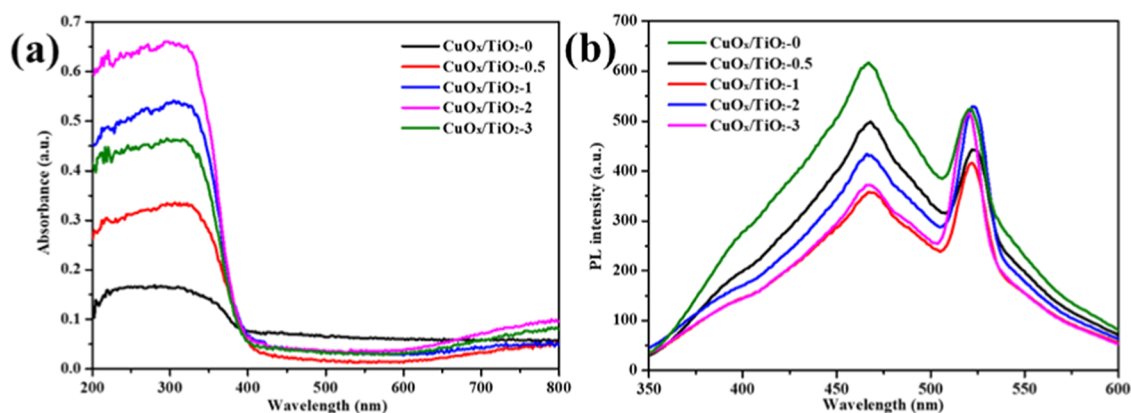**Figure 3.** (a) UV−vis diffuse reflection spectra and (b) PL spectra of the CuO_x/TiO_2 samples.

area and porous structure of the products were evaluated using nitrogen adsorption−desorption measurements (equipment: 3S-2000PSI, BeiShiDe). The X-ray photoelectron spectroscopy (XPS) analysis was carried out using an X-ray photoelectron spectrometer (ESCALAB 250Xi, Thermo Fisher) equipped with monochromatized Al Kα radiation. The binding energy was calibrated using C 1s (284.8 eV) a as reference. Photoluminescence (PL) emission spectra were recorded using a fluorescence spectrophotometer (XRF-1800, SHI-MADZU) with a laser excitation at 300 nm (450 W xenon lamp).

2.4. Measurement of Photocatalytic Activity. The photocatalytic activity of the products was evaluated by the photodegradation of RhB in solution under 300 W xenon lamp (Sirius300PU, $\lambda > 420$ nm) irradiation with a UV-cut filter. Typically, a 50 mg CuO_x/TiO_2 sample was suspended in 100 mL of RhB solution (2×10^{-5} mol L^{-1}) and then stirred for 30 min to achieve the adsorption−desorption equilibrium in the dark. The distance between the lamp and the surface of the liquid was 15 cm. At the defined time, solutions of about 5 mL were taken out and centrifuged to remove the particles. Finally, the concentration of RhB was monitored using an UV−vis spectrophotometer at 554 nm.

3. RESULTS AND DISCUSSION

Figure 1 shows the XRD patterns of unloaded and loaded TiO_2 samples with different amounts of copper. All the diffraction peaks can be well indexed to the anatase phase of TiO_2

(JCPDS 21-1272). The diffraction peaks around $2\theta = 25.3$, 37.7, 48.0, 53.9, and 55.0° can be indexed to the (101), (004), (200), (105), and (211) planes of the anatase titania, respectively.[33,34] This indicates that the loading of copper does not affect the phase of TiO_2, regardless of the amount of the loaded CuO_x. No characteristic diffraction peaks related to CuO_x and other impurities were observed. This may be because the content of CuO_x was low and CuO_x was highly dispersed in TiO_2 particles, and the loaded Cu ions were imbedded into the TiO_2 matrix by occupying the position of Ti atoms.[21] The amplifying diffraction patterns in the 2θ range between 35 and 50° are shown in Figure 1b. It is observed that after loading CuO_x, the diffraction peak intensity of the (004) crystal plane of TiO_2 decreases significantly. The possible reason is that CuO_x anchored in the pore channel could change the X-ray scattering contrast between the pore channels and the walls of mesoporous CuO_x/TiO_2.[34] The average crystal sizes and cell parameters (a, b, c) of the samples before and after loading were calculated using Scherrer's formula, as shown in Table 1. The results demonstrate that the cell volume of TiO_2 increases after loading CuO_x, especially along the c-axis direction. This is because the radius of Cu^{2+} is larger than that of Ti^{4+}, and then, the crystal size increases after Cu^{2+} enters the TiO_2 matrix.

Furthermore, the Raman spectra were analyzed for the samples to study the crystal structure characteristics. As shown in Figure 2, all samples exhibit five Raman active modes located at 141, 197, 394, 516, and 636 cm^{-1} that are identified
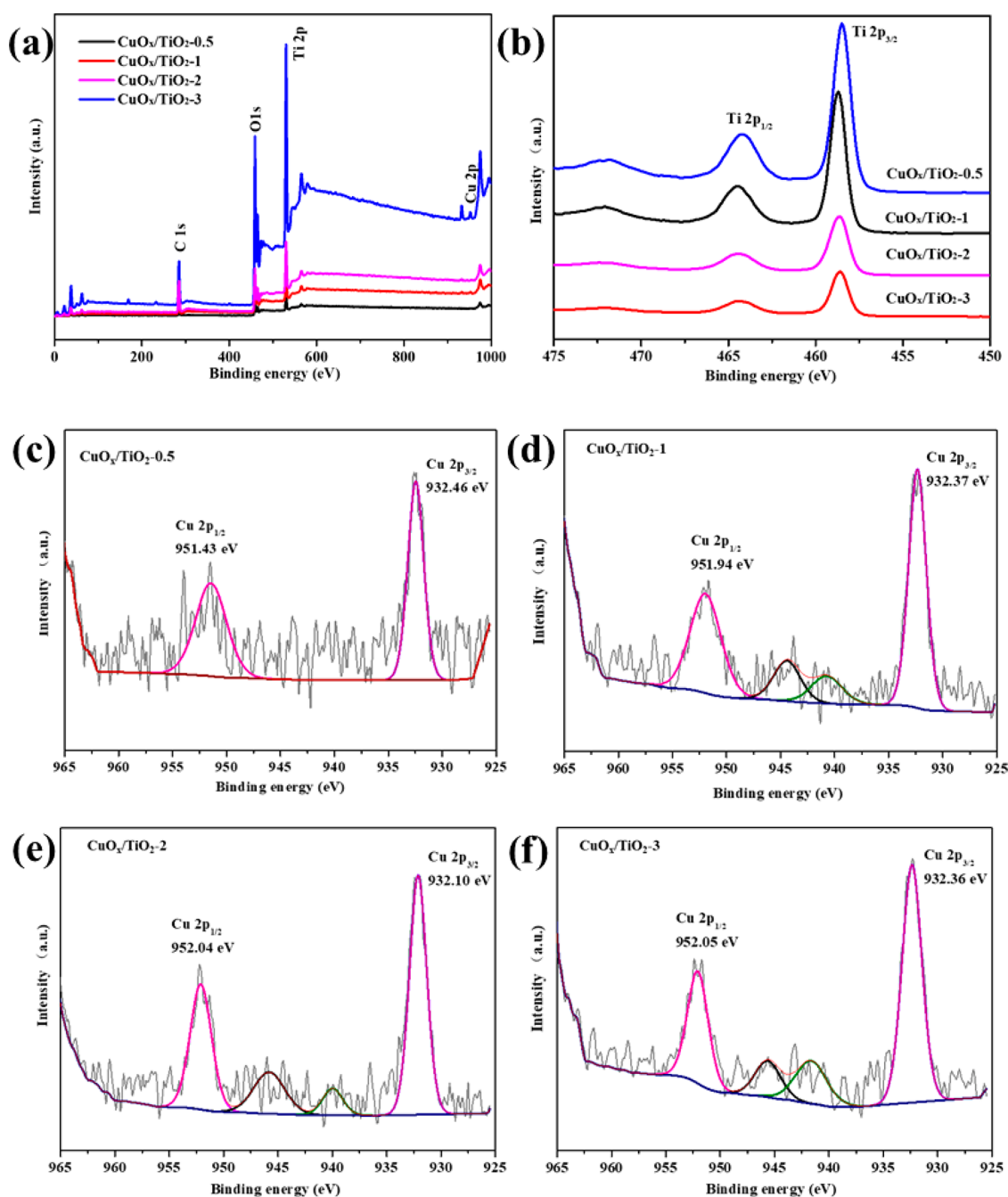
Figure 4. XPS spectra of the CuO$_x$/TiO$_2$ samples and (a) full-range XPS spectra, (b) Ti 2p and (c–f) Cu 2p.

as anatase peaks, which were consistent well with the XRD results.[35] Among them, the E$_g$ peaks at 141, 197, and 636 cm^{-1} correspond to the stretching vibration of O–Ti–O, the B$_{1g}$ peak at 394 cm^{-1} corresponds to the bending vibration of O–Ti–O, and the A$_{1g}$ peak at 516 cm^{-1} corresponds to the antisymmetric bending vibration of O–Ti–O.[36,37] It is worth noting that there are two peaks shifting from 141 and 194 cm^{-1} to 144 and 197 cm^{-1}, respectively, with increasing concentration of Cu.[25] These blue shifts in the peak position indicate that there is an adjustment in the cell size of the CuO$_x$/TiO$_2$ sample.

The UV–vis diffuse reflectance spectra show a significant difference before and after loading copper samples. As shown in Figure 3a, the spectrum of the CuO$_x$/TiO$_2$-0 sample without the Cu loading contains only one absorption peak at

ca. 410 nm, which corresponds to the band-to-band transition of anatase TiO$_2$. The Cu-loaded TiO$_2$ samples exhibit a shoulder peak at ~450 nm except the absorption peak near 410 nm compared to the CuO$_x$/TiO$_2$-0 sample. This shoulder peak is attributed to the existence of Cu, which induces electron transfer from the valence band (VB) of TiO$_2$ to the Cu atom. The broad band at 700–800 nm corresponds to the d–d transition of Cu.[38] According to the absorption spectrum data, the band gaps of all samples were calculated, and the results are shown in Table 1. It can be seen that the band gap of the CuO$_x$/TiO$_2$ sample decreases with increasing amount of the Cu loading. This is helpful for the utilization of solar light.

In addition, the photoluminescence spectra were characterized to understand the impact of the Cu loading on the efficiency of transfer and separation of electrons and holes. As

shown in Figure 3b, there are two emission bands in all spectra. The peaks at around 460 nm in the PL spectra are attributed to the band−band radiation transition, and the peaks at about 520−530 nm are mainly derived from the excitation PL phenomenon.[39,40] The loaded copper has an important effect on the PL intensity of the samples. Once copper is loaded on the Ti^{3+}/TiO_2 sample, the emission intensity of the PL spectra decreases significantly. It is clear that CuO_x/TiO_2-1 has the weakest PL intensity, indicating that it possesses the highest photocharge separation efficiency and the lowest carrier recombination rate.[20] The main reason is that TiO_2 generates photogenerated electrons and holes under photoexcitation. After being loaded with Cu, there is indeed a transfer of electrons from TiO_2 to Cu, preventing the recombination of photogenerated electrons and holes. BET analyses did not evince any significant changes of the CuO_x/TiO_2 co-photo-catalyst with respect to the unloaded Cu sample. All the adsorption−desorption curves can be categorized as IUPAC type III, with the BET surface area ranging between 31and 34 $m^2 \cdot g^{-1}$. All samples showed the characteristics of a mesoporous structure, which is conducive to the adsorption and removal of organic pollutants and makes the photocatalytic reaction easier.

To investigate the valence state of Cu and Ti elements throughout the co-photocatalyst, the CuO_x/TiO_2 samples were characterized by XPS. The survey spectra (Figure 4a) exhibit the characteristic peaks of Cu 2p, Ti 2p, and O 1s, indicating that the Cu element is successfully loaded onto the sample surface. As shown in Figure 4b, the Ti 2p spectra of the samples show two typical peaks located at 458.67 and 464.50 eV, which are assigned to the binding energies of Ti^{4+} $2p_{3/2}$ and Ti^{4+} $2p_{1/2}$, respectively.[15,41,42] Figure 4c−f shows the XPS spectra of Cu 2p. The spectrum of the CuO_x/TiO_2-0.5 sample shows mangy burrs, due to the high background noise caused by the low content of Cu. When the content of Cu is greater than 1%, two characteristic peaks are shown at 951.94 and 932.37 eV, corresponding to the electron binding energies of Cu $2p_{1/2}$ and Cu $2p_{3/4}$ of Cu^0 and Cu^+, respectively, and weak satellite peaks of Cu^+ are also observed at 940−945 eV.[31,43−45] Because CuO_x/TiO_2 was synthesized using Ti^{3+}/TiO_2 as a raw material, Ti^{3+} with strong reducibility would reduce Cu^{2+} to Cu^+ or Cu^0. However, it should be noted that no binding energy peaks of Cu^{2+} near 935 and 955 eV are observed in all the samples, indicating that the Cu species on the samples exist in the form of Cu_2O or Cu rather than as CuO.[46]

The phase structure of the typical sample CuO_x/TiO_2-0.5 was investigated by low- and high-resolution TEM, as shown in Figure 5. The TEM images exhibit a cubic structure with a length of about 50 nm and homogeneous mesoporous structure. The HRTEM images show clearly uniform lattices, which confirm that the sample is highly crystallized. In summary, the morphology and crystal structure of the Ti^{3+}/TiO_2 cube were not changed after Cu loading.[32] To further validate the existence and the content of the loaded Cu on the Ti^{3+}/TiO_2 particles, the samples, CuO_x/TiO_2-N (N = 0.5, 1, 2, 3), were analyzed by EDS (Figure S2 and Table S1), which is a chemical microanalysis technique used together with TEM. When Cu is loaded at less than 1%, the samples CuO_x/TiO_2-0.5 and CuO_x/TiO_2-1 show a homogeneous dispersion of very weak Cu species (Figure 6a,b). With increasing loading content, the CuO_x/TiO_2-2 sample shows a small number of aggregated Cu species (Figure 6c), and the aggregation is more obvious in the CuO_x/TiO_2-3 sample (Figure 6d). It assigns these well-dispersed Cu species as CuO_x clusters consisting of

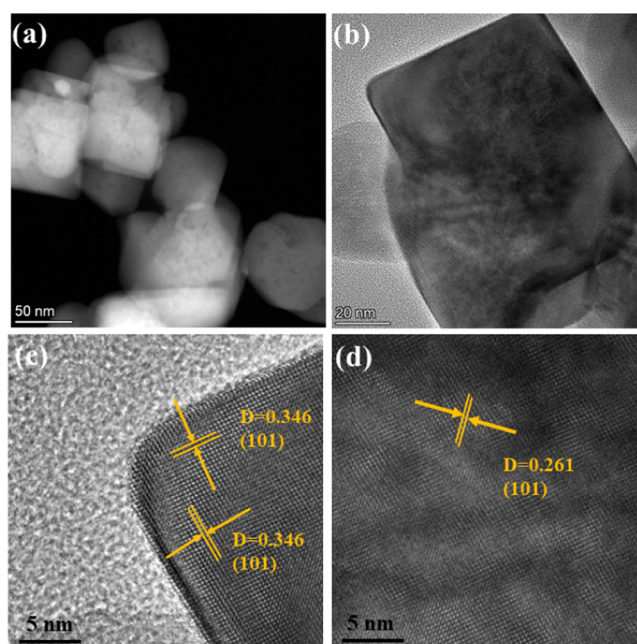**Figure 5.** (a, b) TEM and (c, d) HRTEM images of the CuO_x/TiO_2-0.5 sample.

about 2−3 nm nanocrystals. It has been reported that CuO_x clusters are attached to the surface of TiO_2 through the combination of O atoms and unsaturated 5C-Ti atoms.[22]

The full spectral light and visible light photocatalytic activities of the co-photocatalysts were evaluated by RhB degradation to explore the effect of the Cu loading. For comparison, commercial nano-TiO_2 (P25) was also tested under the same conditions. Figure 7a,b shows the photo-degradation activities versus Cu loading quantity under full spectral light irradiation. It can be seen that the loaded Cu has a great influence on the photocatalytic activities of the co-photocatalyst. The sample CuO_x/TiO_2-1 demonstrates strong photocatalytic activity with a RhB degradation rate of 99% after 20 min, which is similar to that of P25. The photodegradation constants within the first 20 min were calculated, in the following order: P25 ($K = 0.391$ min^{-1}) > CuO_x/TiO_2-1 ($K = 0.283$ min^{-1}) > CuO_x/TiO_2-0.5 ($K = 0.264$ min^{-1}) > CuO_x/TiO_2-2 ($K = 0.041$ min^{-1}) > CuO_x/TiO_2-3 ($K = 0.040$ min^{-1}). It can be seen from Figure 7e that with the increase of the photodegradation reaction time, the absorption peak of RhB aqueous solution blue-shifts gradually from 554 to 532 nm. At the same time, the color of the reaction suspension gradually changes from red to light pink and finally becomes transparent. This is because the conjugated structure of RhB was destroyed to form N,N,N triethyl rhodamine (TER) with the absorption peak at 532 nm.[47]

The photocatalytic activities of the samples under visible light exhibit a increase first followed by a decline with increasing amounts of the Cu loading, and the optimum amount of Cu loading is 1.0%, as shown in Figure 7c,d. Different from the results under full spectral light irradiation, the photodegradation performance of CuO_x/TiO_2-1 is higher than that of P25, and its apparent reaction rate constant is 1.5 times greater than that of P25. The results of these comparative experiments indicate that the spectral response range of Cu-loaded TiO_2 is widened, which leads to the
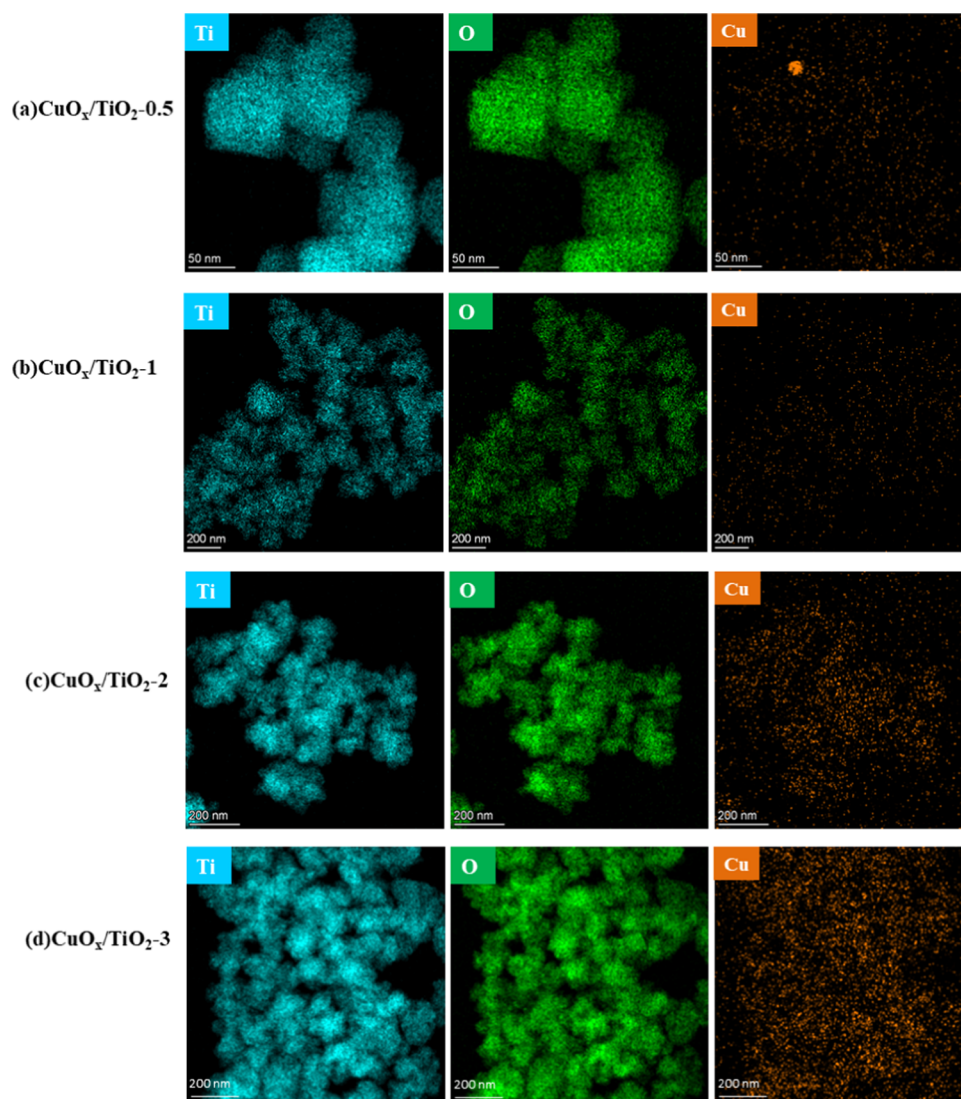
Figure 6. EDS mapping of the CuO_x/TiO_2 samples, (a) CuO_x/TiO_2-0.5; (b) CuO_x/TiO_2-1; (c) CuO_x/TiO_2-2; and (d) CuO_x/TiO_2-3.

enhanced photocatalytic activity. However, there is an optimal Cu loading amount, and when the loading amount is less than the optimal value, the Cu species can trap electrons to inhibit the photogenerated electron−hole recombination, and then, the catalytic activity increases with the increase in the loading amount of Cu. On the contrary, the high concentration of CuO_x species may cover the light irradiation on the TiO_2 surface and can also act as recombination centers of photogenerated electron−hole pairs.[31] Furthermore, to understand the reusable nature of the co-photocatalyst, repeating experiments were carried out on CuO_x/TiO_2-1. As shown in Figure 8a,b, the CuO_x/TiO_2-1 exhibited excellent stability both under the full spectral and UV light irradiation during five continuous cycles. The main reason is that the organic dye material adsorbed on the surface of the sample falls off after repeated washing.[48]

The effects of different copper precursors and the TiO_2 substrate on the photocatalytic activity were also discussed (Figures S3 and S4). The results show that the sample synthesized using $Cu(NO_3)_2$ exhibited the highest photocatalytic activity under both visible light irradiation and full spectral light irradiation. Especially under visible light, the photodegradation rate constants of the sample synthesized

using $Cu(NO_3)_2$ (K = 0.012 min^{-1}) are 7.5 and 6.7 times those of the sample synthesized using $Cu(OAc)_2$ (K = 0.0016 min^{-1}) and $CuSO_4$ (K = 0.0018 min^{-1}), respectively. As shown in Figure S3c, characteristic peaks at 934.24 and 954.58 eV, corresponding to the electron binding energies of Cu^{2+} $2p_{3/2}$ and Cu^{2+} $2p_{1/2}$, respectively, and a satellite peak at 943.33 eV are observed, indicating that the Cu species on the sample synthesized using P25 exist in the form of CuO. The photodegradation activity of the sample ($P25 + Cu(NO_3)_2$) synthesized using P25 is lower than that of the sample synthesized using Ti^{3+}/TiO_2 under visible light irradiation (Figure S4c,d). These results further confirm the beneficial effect of the valence state of Cu species on charge transfer in photocatalytic processes.

To further investigate the photodegradation mechanism, capture experiments of the active substances were carried out on CuO_x/TiO_2-1. As shown in Figure 9, after adding IPA and EDTA-2Na, the photodegradation rate of RhB decreased sharply, while that of AgNO3 was moderate. During photocatalysis, EDTA-2Na and IPA act as a hole-trapping agent and a hydroxyl scavenger, respectively, and AgNO3 is used as an electron-trapping agent.[49,50] The result indicates that holes and hydroxyl radicals play major roles and electrons play a
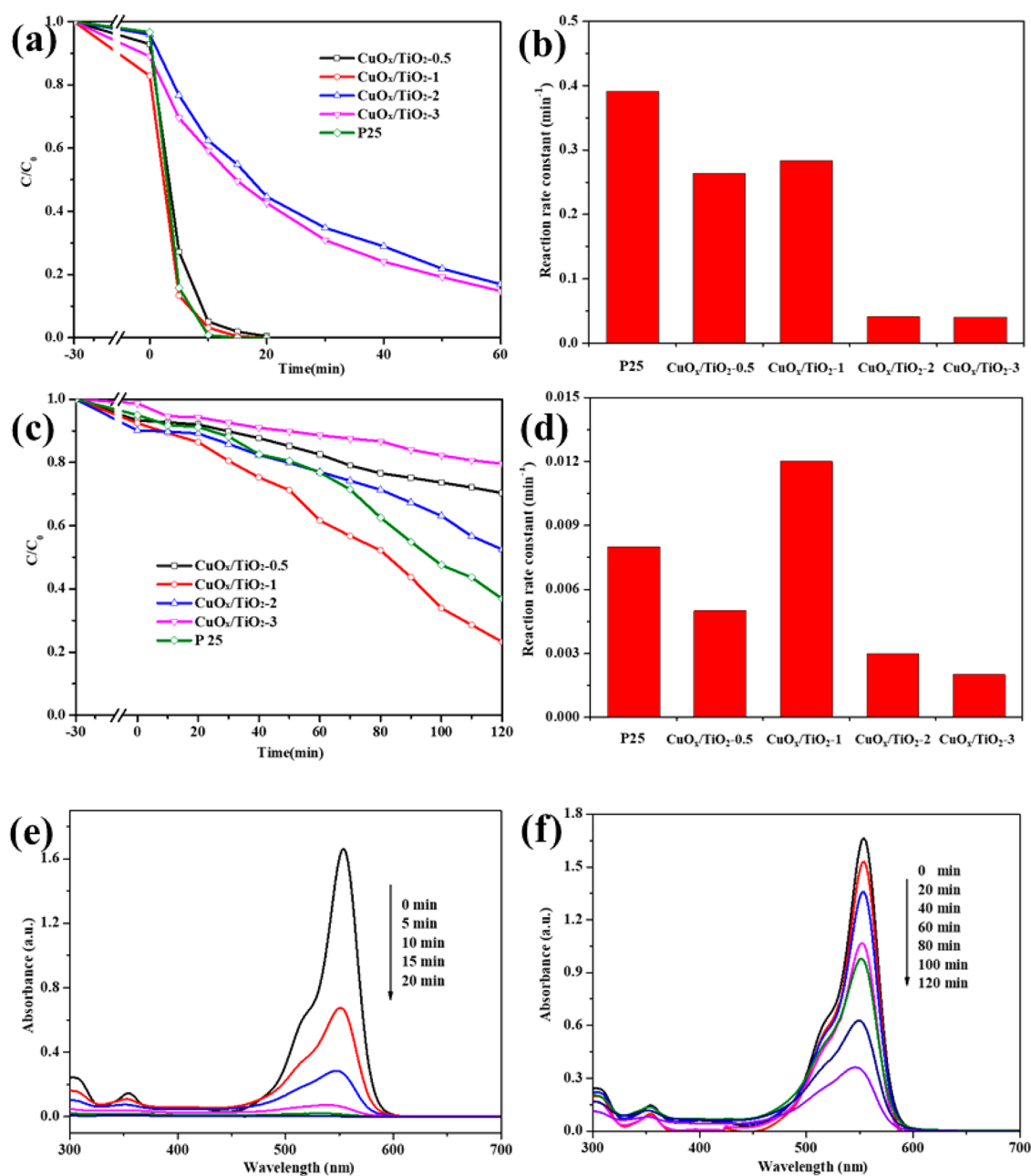
Figure 7. (a, b) Photocatalytic activities and reaction rate constant of the CuO$_x$/TiO$_2$ samples for the RhB degradation (under full spectral light); (c, d) photocatalytic activities and reaction rate constant of the CuO$_x$/TiO$_2$ samples for the RhB degradation (under visible light); and (e) UV−vis spectrum changes of RhB over CuO$_x$/TiO$_2$-1 (under full spectral light) and (f) under visible light.

supplementary role in photocatalysis. Loading Cu could produce the d-orbital underneath the CB of TiO$_2$ and as a result could enhance the visible light response. On the other hand, the CuO$_x$ clusters on the surface of the CuO$_x$/TiO$_2$ co-photocatalyst exhibit high reversibility between Cu$^+$ and Cu^0, which can promote the electron migration greatly. This can prevent the recombination of the photogenerated electron−hole pairs and thus efficiently prolong the hole life.[34] The photogenerated holes that have strong oxidability can react with the adsorbed H$_2$O to form hydroxyl radicals ($^\bullet$OH), and the photogenerated electrons are trapped by O$_2$ to form reactive oxygen species ($^\bullet$O$_2$). These crucial reactive species destroy the molecular structure of RhB, oxidizing it into CO$_2$ and H$_2$O.

4. CONCLUSIONS

CuO$_x$/TiO$_2$ co-photocatalysts were synthesized using a mesoporous Ti^{3+}/TiO$_2$ cube as a substrate by an impregnation method, in which CuO$_x$ clusters with 2−3 nm nanocrystals were loaded uniformly on the TiO$_2$ cube. They exhibited excellent photodegradation performance toward RhB under visible light illumination. Among all samples, CuO$_x$/TiO$_2$-1 exhibited the highest photodegradation efficiency, which was 1.5 times higher than that of the commercial nano-TiO$_2$ P25. During the co-photocatalyst synthesis process, the uniform mesoporous structure of the substrate greatly improved the uniformity of the loaded Cu, and the valence state of the loaded Cu atoms was changed by the Ti^{3+} defects in the Ti^{3+}/TiO$_2$ substrate. This valence change promoted photogenerated
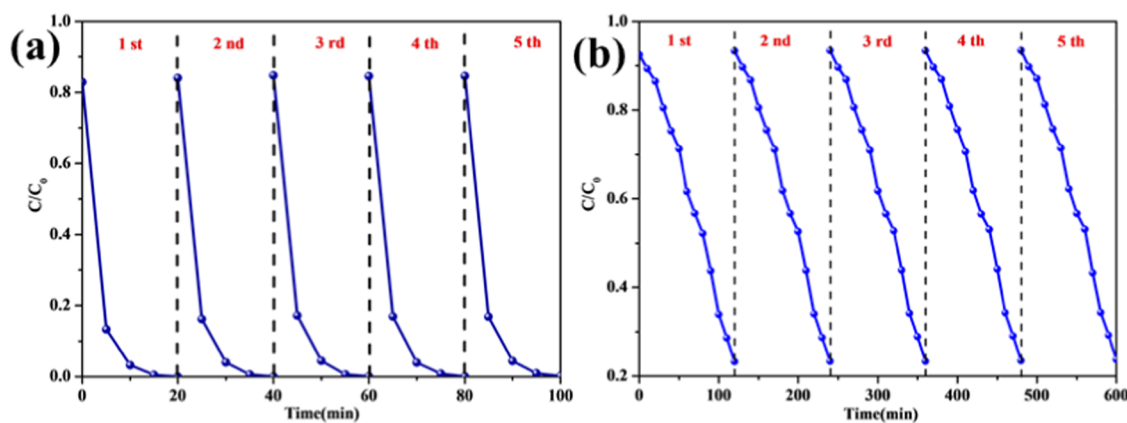
Figure 8. (a) Repetitive test curves of CuO_x/TiO_2-1 under full spectral light and (b) repetitive test curves of CuO_x/TiO_2-1 under visible light.

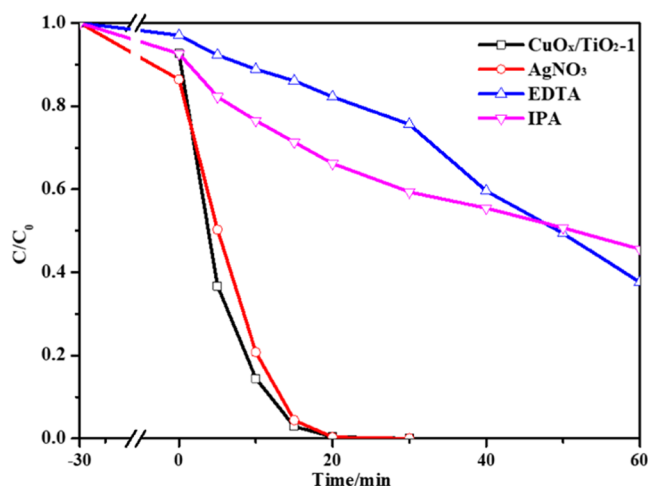**Figure 9.** Photocatalytic activity of CuO_x/TiO_2-1 after adding different trapping agents.

electron transfer from the TiO_2 CB to the CuO_x species. Furthermore, it demonstrated that the synergistic effect between the CuO_x species and TiO_2 was also the reason for enhancement of the photocatalytic activity of the co-photocatalyst. Therefore, the cooperative interaction between the loaded metal and the oxygen defects should not be overlooked in the design of heterogeneous catalyst structures.

■ ASSOCIATED CONTENT

ⓢ Supporting Information

The Supporting Information is available free of charge at https://pubs.acs.org/doi/10.1021/acsomega.2c07364.

> N_2 adsorption−desorption isotherms and the corresponding pore size distribution of the CuO_x/TiO_2 samples, EDS spectrum and the mass ratio of different elements of the CuO_x/TiO_2 samples, Cu 2p XPS spectra of the samples synthesized with different precursors, and photocatalytic activities and reaction rate constant of the samples synthesized with different precursors for the RhB degradation (PDF)

■ AUTHOR INFORMATION

Corresponding Author

Li Li − *College of Chemistry and Chemical Engineering, Chongqing University of Technology, Chongqing 400054, China*; ⓘ orcid.org/0000-0002-1272-0342; Email: chenlili@cqut.edu.cn

Authors

Xinhong Chen − *Pangang Group Vanadium & Titanium Resources Co., Ltd., Panzhihua 617000, China*

Xuejun Quan − *College of Chemistry and Chemical Engineering, Chongqing University of Technology, Chongqing 400054, China*

Facheng Qiu − *College of Chemistry and Chemical Engineering, Chongqing University of Technology, Chongqing 400054, China*

Xingran Zhang − *College of Chemistry and Chemical Engineering, Chongqing University of Technology, Chongqing 400054, China*; ⓘ orcid.org/0000-0001-6186-9613

Complete contact information is available at:
https://pubs.acs.org/10.1021/acsomega.2c07364

Notes

The authors declare no competing financial interest.

■ ACKNOWLEDGMENTS

■ REFERENCES

(1) Fujishima, A.; Honda, K. Electrochemical photolysis of water at a semiconductor electrode. *Nature* **1972**, *238*, 37−38.

(2) Li, W.; Elzatahry, A.; Aldhayan, D.; Zhao, D. Y. Core−shell structured titanium dioxide nanomaterials for solar energy utilization. *Chem. Soc. Rev.* **2018**, *47*, 8203−8237.

(3) Shayegan, Z.; Lee, C. S.; Haghighat, F. TiO_2 photocatalyst for removal of volatile organic compounds in gas phase − a review. *Chem. Eng. J.* **2018**, *334*, 2408−2439.

(4) Sabri, M.; Habibi-Yangjeh, A.; Pouran, S. R.; Wang, C. Titania-activated persulfate for environmental remediation: the-state-of-the-art. *Catal. Rev.* **2021**, DOI: 10.1080/01614940.2021.1996776.

(5) Akhundi, A.; Badiei, A.; Ziarani, G. M.; Habibi-Yangjeh, A.; Munoz-Batista, M. J.; Luque, R. Graphitic carbon nitride-based photocatalysts: toward efficient organic transformation for value-added chemicals production. *Mol. Catal.* **2020**, *488*, No. 110902.

(6) Yu, J.; Low, J.; Xiao, W.; Zhou, P.; Jaroniec, M. Enhanced photocatalytic CO_2-reduction activity of anatase TiO_2 by coexposed {001} and {101} facets. *J. Am. Chem. Soc.* **2014**, *136*, 8839−8842.

(7) Eskandarloo, H.; Zaferani, M.; Kierulf, A.; Abbaspourrad, A. Shape-controlled fabrication of TiO_2 hollow shells toward photocatalytic application. *Appl. Catal., B* **2018**, *227*, 519−529.

(8) Akhundi, A.; Habibi-Yangjeh, A.; Abitorabi, M.; Pouran, S. R. Review on photocatalytic conversion of carbon dioxide to value-added compounds and renewable fuels by graphitic carbon nitride-based photocatalysts. *Catal. Rev.* **2019**, *61*, 595−628.

(9) Li, B.; Zeng, H. C. Architecture and preparation of hollow catalytic devices. *Adv. Mater.* **2018**, *31*, No. 1801104.

(10) Akhundi, A.; Moshfegh, A. Z.; Habibi-Yangjeh, A.; Sillanpää, M. Simultaneous dual-functional photocatalysis by g-C_3N_4-based nanostructures. *ACS ES&T Eng.* **2022**, *2*, 564−585.

(11) Joo, J. B.; Dahl, M.; Li, N.; Zaera, F.; Yin, Y. D. Tailored synthesis of mesoporous TiO_2 hollow nanostructures for catalytic applications. *Energy Environ. Sci.* **2013**, *6*, 2082−2092.

(12) Le, Z.; Liu, F.; Nie, P.; Li, X.; Liu, X.; Bian, Z.; Chen, G.; Wu, H. B.; Lu, Y. Pseudocapacitive sodium storage in mesoporous single-crystal-like TiO_2−graphene nanocomposite enables high-performance sodium-ion capacitors. *ACS Nano* **2017**, *11*, 2952−2960.

(13) Wang, J.; Tafen, D. N.; Lewis, J. P.; Hong, Z.; Manivannan, A.; Zhi, M.; Li, M.; Wu, N. Origin of photocatalytic activity of nitrogen-doped TiO_2 nanobelts. *J. Am. Chem. Soc.* **2009**, *131*, 12290−12297.

(14) Zuo, F.; Wang, L.; Wu, T.; Zhang, Z.; Borchardt, D.; Feng, P. Self-doped Ti^{3+} enhanced photocatalyst for hydrogen production under visible light. *J. Am. Chem. Soc.* **2010**, *132*, 11856−11857.

(15) Wang, Y.; Yang, C.; Chen, A.; Pu, W.; Gong, J. Influence of yolk-shell Au@TiO_2 structure induced photocatalytic activity towards gaseous pollutant degradation under visible light. *Appl. Catal., B* **2019**, *251*, 57−65.

(16) Geng, R.; Yin, J.; Zhou, J.; Jiao, T.; Feng, Y.; Zhang, L.; Chen, Y.; Bai, Z.; Peng, Q. In situ construction of Ag/TiO_2/g-C_3N_4 heterojunction nanocomposite based on hierarchical co-assembly with sustainable hydrogen evolution. *Nanomaterials* **2020**, *10*, 1.

(17) Melvin, A. A.; Illath, K.; Das, T.; Raja, T.; Bhattacharyya, S.; Gopinath, C. M−Au/TiO_2 (M = Ag, Pd, and Pt) nanophoto catalyst for overall solar water splitting: role of interfaces. *Nanoscale* **2015**, *7*, 13477−13488.

(18) Liang, S.; Deng, X.; Xu, G.; Xiao, X.; Wang, M.; Guo, X.; Ma, P.; Cheng, Z.; Zhang, D.; Lin, J. A Novel Pt−TiO_2 Heterostructure with oxygen-deficient layer as bilaterally enhanced sonosensitizer for synergistic chemo-sonodynamic cancer therapy. *Adv. Funct. Mater.* **2020**, *30*, No. 1908598.

(19) DeRita, L.; Dai, S.; Lopez-Zepeda, K.; Pham, N.; Graham, G. W.; Pan, X.; Christopher, P. Catalyst architecture for stable single atom dispersion enables site-specific spectroscopic and reactivity measurements of CO adsorbed to Pt atoms, oxidized Pt clusters, and metallic Pt clusters on TiO_2. *J. Am. Chem. Soc.* **2017**, *139*, 14150−14165.

(20) Lee, B. H.; Park, S.; Kim, M.; Sinha, A. K.; Lee, S. C.; Jung, E.; Chang, W. J.; Lee, K. S.; Kim, J. H.; Cho, A.; Kim, H.; Nam, K. T.; Hyeon, T. Reversible and cooperative photoactivation of single-atom Cu/TiO_2 photocatalysts. *Nat. Mater.* **2019**, *18*, 620−626.

(21) Docao, S.; Koirala, A. R.; Kim, M. G.; Hwang, I. C.; Song, M. K.; Yoon, K. B. Solar photochemical−thermal water splitting at 140 °C with Cu-loaded TiO_2. *Energy Environ. Sci.* **2017**, *10*, 628−640.

(22) Dozzi, M. V.; Chiarello, G. L.; Pedeoni, M.; Livraghi, S.; Giamello, E.; Selli, E. High photocatlytic hydrogen production on Cu (II) pre-grafted Pt/TiO_2. *Appl. Catal., B* **2017**, *209*, 417−428.

(23) Yuan, Y.; Sheng, K.; Zeng, S.; Han, X.; Sun, L.; Lončarić, I.; Zhan, W.; Sun, D. Engineering Cu/TiO_2@N-Doped C interfaces derived from an atom-precise heterometallic $Cu_4^{II}Ti_5^{IV}$ cluster for efficient photocatalytic hydrogen evolution. *Inorg. Chem.* **2020**, *59*, 5456−5462.

(24) Wang, R. Y.; Wang, J. X.; Jia, J. F.; Wu, H. S. The growth pattern and electronic structures of Cu_n(n = 1−14) clusters on rutile TiO_2(110) surface. *Appl. Surf. Sci.* **2021**, *536*, No. 147793.

(25) Alotaibi, A. M.; Williamson, B. A. D.; Sathasivam, S.; Kafizas, A.; Alqahtani, M.; Vazquez, C. S.; Buckeridge, J.; Wu, J.; Nair, S. P.; Scanlon, D. O.; Parkin, I. P. Enhanced photocatalytic and antibacterial ability of Cu-doped anatase TiO_2 thin films: theory and experiment. *ACS Appl. Mater. Interfaces* **2020**, *12*, 15348−15361.

(26) Gu, W.; Lu, F.; Wang, C.; Kuga, S.; Wu, L.; Huang, Y.; Wu, M. Face-to-face interfacial assembly of ultrathin g-C_3N_4 and anatase TiO_2 nanosheets for enhanced solar photocatalytic activity. *ACS Appl. Mater. Interfaces* **2017**, *9*, 28674−28684.

(27) Liu, L.; Chen, X. Titanium dioxide nanomaterials: self-structural modifications. *Chem. Rev.* **2014**, *114*, 9890−9918.

(28) Zhang, H.; Cai, J.; Wang, Y.; Wu, M.; Meng, M.; Tian, Y.; Li, X.; Zhang, J.; zheng, L.; Jiang, Z.; Gong, J. Insights into the effects of surface/bulk defects on photocatalytic hydrogen evolution over TiO_2 with exposed {001} facets. *Appl. Catal., B* **2018**, *220*, 26−136.

(29) Chen, Y.; Zhang, X.; Wang, L.; Cheng, X.; Shang, Q. Rapid removal of phenol/antibiotics in water by Fe-(8-hydroxyquinoline-7-carboxylic)/TiO_2 flower composite: Adsorption combined with photocatalysis. *Chem. Eng. J.* **2020**, *402*, No. 126260.

(30) Park, S. M.; Razzaq, A.; Park, Y. H.; In, S.; et al. Hybrid Cu_xO−TiO_2 heterostructured composites for photocatalytic CO_2 reduction into methane using solar irradiation: sunlight into fuel. *ACS Omega* **2016**, *1*, 868−875.

(31) Li, Y.; Wang, W. N.; Zhan, Z.; Woo, M. H.; Wu, C. Y.; Biswas, P. Photocatalytic reduction of CO_2 with H_2O on mesoporous silica supported Cu/TiO_2 catalysts. *Appl. Catal., B* **2010**, *100*, 386−392.

(32) Li, L.; Chen, X. H.; Wang, L.; Tao, C. Y.; Wu, X. P.; Du, J.; Liu, Z. H. Synthesis of Ti^{3+} self-doped mesoporous TiO_2 cube with enhanced visible-light photoactivity by a simple reduction method. *J. Alloys Compd.* **2020**, *845*, No. 156138.

(33) Mino, L.; Pellegrino, F.; Rades, S.; Steffi, R.; Dan, H. V.; Giuseppe, S.; Valter, M.; Gianmario, M. Beyond shape engineering of TiO_2 nanoparticles: post-synthesis treatment dependence of surface hydration, hydroxylation, lewis acidity and photocatalytic activity of TiO_2 anatase nanoparticles with dominant {001} or {101} facets. *ACS Appl. Mater. Interfaces* **2018**, *1*, 5355−5365.

(34) Xu, T. Z.; Zheng, H.; Zhang, P. Y. Isolated Pt single atomic sites anchored on nanoporous TiO_2 film for highly efficient photocatalytic degradation of low concentration toluene. *J. Hazard. Mater.* **2020**, *388*, No. 121746.

(35) Xin, X. Y.; Xu, T.; Yin, J.; Wang, L.; Wang, C. Management on the location and concentration of Ti^{3+} in anatase TiO_2 for defects-induced visible-light photocatalysis. *Appl. Catal., B* **2015**, *176*−*177*, 354−362.

(36) Balaganapathi, T.; Kaniamuthan, B.; Vinoth, S.; Thilakan, P. PEG assisted synthesis of porous TiO_2 using sol-gel processing and its characterization studies. *Mater. Chem. Phys.* **2017**, *189*, 50−55.

(37) Xia, T.; Zhang, Y.; Murowchick, J.; Chen, X. Vacuum-treated titanium dioxide nanocrystals: Optical properties, surface disorder, oxygen vacancy, and photocatalytic activities. *Catal. Today* **2014**, *225*, 2−9.

(38) Chen, M.; Wang, H.; Chen, X.; Wang, F.; He, H.; et al. High-performance of Cu-TiO_2 for photocatalytic oxidation of formaldehyde under visible light and the mechanism study. *Chem. Eng. J.* **2020**, *390*, No. 124481.

(39) Yang, L.; Xu, L.; Bai, X.; Jin, P. Enhanced visible-light activation of persulfate by Ti^{3+} self-doped TiO_2/graphene nanocomposite for the rapid and efficient degradation of micropollutants in water. *J. Hazard. Mater.* **2019**, *365*, 107−117.

(40) Zhang, C.; Tian, L.; Chen, L.; Li, X.; Lv, K.; Deng, K. One-pot topotactic synthesis of Ti^{3+} self-doped 3D TiO_2 hollow nanoboxes with enhanced visible light response. *Chin. J. Catal.* **2018**, *39*, 1373−1383.

(41) Li, L.; Wang, L.; Chen, X. H.; Tao, C. Y.; Du, J.; Liu, Z. H. The synthesis of bayberry- like mesoporous TiO_2 microspheres by a kinetics-controlled method and their hydrophilic films. *CrystEngComm* **2020**, *22*, 969−978.

(42) Hu, W.; Zhou, W.; Zhang, K.; Zhang, X.; Wang, L.; Jiang, B.; Tian, G.; Zhao, D.; Fu, H. Facile strategy for controllable synthesis of stable mesoporous black TiO_2 hollow spheres with efficient solar-driven photocatalytic hydrogen evolution. *J. Mater. Chem. A* **2016**, *4*, 7495−7502.

(43) Pham, T.-D.; Lee, B. Novel photocatalytic activity of Cu@V co-doped TiO_2/PU for CO_2 reduction with H_2O vapor to produce solar fuels under visible light. *J. Catal.* **2017**, *345*, 87−95.

(44) Zhang, X.; Yu, Y.; Jiang, D.; Jiao, Y.; Wu, Y.; Peng, Z.; Zhou, J.; Wu, J.; Dong, Z. Synthesis and characterization of a bi-functional hydroxyapatite/Cu-doped TiO_2 composite coating. *Ceram. Int.* **2019**, *45*, 6693−6701.

(45) She, H.; Zhao, Z.; Bai, W.; Huang, J.; Wang, L.; Wang, Q. Enhanced performance of photocatalytic CO_2 reduction via synergistic effect between chitosan and $Cu:TiO_2$. *Mater. Res. Bull.* **2020**, *124*, No. 110758.

(46) Zhang, X.; Peng, Z.; Lu, X.; Lv, Y.; Cai, G.; Yang, L.; Dong, Z. Microstructural evolution and biological performance of Cu-incorporated TiO_2 coating fabricated through one-step micro-arc oxidation. *Appl. Surf. Sci.* **2020**, *508*, No. 144766.

(47) Wang, J. G.; He, B.; Kong, X. Z. A study on the preparation of floating photocatalyst supported by hollow TiO_2 and its performance. *Appl. Surf. Sci.* **2015**, *327*, 406−412.

(48) Yang, X.; Cui, H.; Li, Y.; Qin, J.; Zhang, R.; Hua, T. Fabrication of Ag_3PO_4-Graphene Composites with Highly Efficient and Stable Visible Light Photocatalytic Performance. *ACS Catal.* **2013**, *3*, 363−369.

(49) Yang, X.; Qin, J.; Jiang, Y.; Li, R.; Li, Y.; Tang, H. Bifunctional TiO_2/Ag_3PO_4/graphene composites with superior visible light photocatalytic performance and synergistic inactivation of bacteria. *RSC Adv.* **2014**, *4*, 18627−18636.

(50) Wang, P.; Jia, C.; Li, J.; Yang, P. Ti^{3+}-doped TiO_2(B)/anatase spheres prepared using thioglycolic acid towards super photocatalysis performance. *J. Alloys Compd.* **2019**, *780*, 660−670.